Journal of Science: Advanced Materials and Devices 6 (2021) 587–594

Contents lists available at ScienceDirect

Journal of Science: Advanced Materials and Devices

journal homepage: www.elsevier.com/locate/jsamd

Original Article

Enhanced magnetocaloric performance in nanocrystalline/amorphous $Gd_3Ni/Gd_{65}Ni_{35}$ composite microwires

Y.F. Wang [a, b], Y.Y. Yu [b], H. Belliveau [b], N.T.M. Duc [c, ****], H.X. Shen [d, ***], J.F. Sun [d], J.S. Liu [e], F.X. Qin [a, **], S.C. Yu [f], H. Srikanth [b], M.H. Phan [b, *]

[a] Institute for Composites Science Innovation (InCSI), School of Materials Science and Engineering, Zhejiang University, 38 Zheda Road, Hangzhou, 310027, PR China
[b] Department of Physics, University of South Florida, Tampa, FL, 33620, USA
[c] The University of Danang, University of Science and Education, 459 Ton Duc Thang, Lien Chieu, Danang, Viet Nam
[d] School of Materials Science and Engineering, Harbin Institute of Technology, Harbin, 150001, China
[e] School of Materials Science and Engineering, Inner Mongolia University of Technology, Hohhot, 010051, PR China
[f] School of Natural Science, Ulsan National Institute of Science and Technology, Ulsan, 44919, South Korea

ARTICLE INFO

Article history:
Received 24 June 2021
Received in revised form
27 July 2021
Accepted 30 July 2021
Available online 10 August 2021

Keywords:
Melt-extraction
Microwire
Magnetocaloric effect
Magnetic refrigeration

ABSTRACT

A novel class of nanocrystalline/amorphous $Gd_3Ni/Gd_{65}Ni_{35}$ composite microwires were created directly from melt-extraction through controlled solidification. X-ray diffraction (XRD), transmission electron microscopy (TEM), and selected area electron diffraction (SAED) confirmed the formation of a biphase nanocrystalline/amorphous structure in these wires. Magnetic and magnetocaloric experiments indicate a large magnetic entropy change ($-\Delta S_M$ ~9.64 J/kg K), large refrigerant capacity (*RC* ~742.1 J/kg), and large maximum adiabatic temperature change (ΔT_{ad}^{max}~5 K) around the Curie temperature of ~120 K for a field change of 5 T. These values are ~1.5 times larger relative to its bulk counterpart and are superior to other candidate materials being considered for active magnetic refrigeration in the liquid nitrogen temperature range.

1. Introduction

Magnetic refrigeration (MR) technology based on the magnetocaloric effect (MCE) has opened a promising chapter in the future of cooling as it may one day be able to replace conventional gas compression (CGC) commonly used in today's refrigeration devices. Higher cooling efficiency, compactness, and environmental friendliness are some of the outstanding advantages of MR technology compared to CGC technology [1–3]. Since MR uses a magnetic solid-state substance as the refrigerant in cooling devices, the emerging question is how to design and fabricate a solid-state material with not only a large MCE but also practical applicability. Based on the main criteria used to evaluate the MCE effect and its usefulness in MR, including the adiabatic temperature change (ΔT_{ad}), the magnetic entropy change (ΔS_M), and the refrigerant capacity (RC) [4–7], the lanthanide element Gadolinium (Gd) is being tapped as the best candidate for use in sub-room-temperature magnetic refrigerators, and, more importantly, this material undergoes a second-order magnetic transition (SOMT) [3]. However, pure Gd is very expensive and challenging to fabricate into practical shapes as a refrigerant in an active magnetic refrigerator (AMR). A natural solution to this issue is to alloy Gd with other components, such as ferromagnetic elements (Fe, Co, Ni …), soft-magnetic components (CoFeSiB), or non-magnetic components (SiB). Furthermore, detailed analyses on the advantages and disadvantages of different alloyed magnetic refrigerants (Gd_5T_4,

* Corresponding author.
** Corresponding author.
*** Corresponding author. Department of Physics, University of South Florida, Tampa, FL, 33620, USA.
**** Corresponding author.
E-mail addresses: duc.physics@gmail.com (N.T.M. Duc), hitshenhongxian@163.com (H.X. Shen), faxiangqin@zju.edu.cn (F.X. Qin), phanm@usf.edu (M.H. Phan).
Peer review under responsibility of Vietnam National University, Hanoi.

https://doi.org/10.1016/j.jsamd.2021.07.010

Gd_7T_3, $REMnO_3$, LaFeSi, MnAs, FeMnPAs, etc.) have shown the superior properties of Gd-based alloys for use in AMRs [8].

MCE research on Gd-based materials has largely progressed in various forms of bulk metallic glasses (BMGs) and amorphous particles, thin films, ribbons, and microwires for the last 15 years [9–33]. The number of studies conducted on Gd-based glass ribbons and microwires [12–33] is much higher than that of other Gd-based material forms [9–11]. Contrary to BMGs, thin films, and ribbons, a cooling device using microwires would permit their utilization in miniature refrigeration systems. The cooling efficiency in such systems considers a combination of the device's cooling power and the operating frequency. Theory predicts that reducing the dimensions of a magnetic refrigerator can increase the device's cooling power by increasing the operating frequency. Indeed, it has been theoretically and experimentally shown that, in comparison with other shapes (ribbons, films, BMGs …), magnetocaloric materials in microwire form maintain an enhanced cooling efficiency due to achieving the highest operating frequency [9–33]. Furthermore, these magnetocaloric microwires can give rise to a larger heat transfer between the magnetic refrigerant and surrounding liquid because of the microwire's large surface areas [34], which make them an ideal candidate for use in AMRs [35]. For example, the RC value of a $Gd_{53}Al_{24}Co_{20}Zr_3$ microwire (687 K kg^{-1} [32]) is significantly higher than that of its BMG counterpart (509 K kg^{-1} [9]) at $\mu_0 H = 5$ T.

Recently, our group has reported on a large class of Gd-based microwire candidates fabricated by a modified precision melt-extraction method that possess excellent mechanical and magnetocaloric properties appropriate for use in AMRs [15–33]. Relative to their bulk counterparts, these microwires have shown larger ΔS_M and RC values. In the past, Gd has been alloyed with different components such as Gd-AlCo [20–23,31], Gd-CoFeSiB [24,26], Gd-FeAl [25,27], Gd-AlCoZr [15–17,32], Gd–Ni [17], and Gd-SiB [33] with the goal to enhance the MCE and RC of melt-extracted microwires. A relatively simple but highly effective method to improve MCE and RC performances is through annealing (or heat treatment) of amorphous Gd-based microwires. Belliveau *et al.* [32] demonstrated that low temperatures and short annealing times of $Gd_{53}Al_{24}Co_{20}Zr_3$ amorphous microwires can generate nanocrystals embedded in an amorphous matrix that significantly enhance both the ΔS_M and RC values, as well as improve the mechanical response of the microwire due to partially released stresses during the annealing process. However, a biphase nanocrystalline/amorphous structured microwire can also be created through a controlled melt-extraction process without annealing treatment, which has been demonstrated in Gd-Co-Al alloy microwires by our group [31]. The presence of a ~20% volume fraction of 10-nm nanocrystals embedded in an amorphous matrix yielded an excellent magnetocaloric response with large values of -ΔS_M ~9.7 J kg^{-1} K^{-1}, ΔT_{ad} ~5.2 K, and RC ~654 J kg^{-1} for a field change of 5 T [31].

Furthermore, Phan *et al.* showed that reducing the size of antiferromagnetic (AFM) particles in a multi-phase magnetic material to the nanoscale could significantly weaken AFM coupling and allow a moderate applied magnetic field to overcome AFM coupling to become ferromagnetically (FM) ordered, thus enhancing the MCE and RC values of the material [36]. Our group has directly fabricated antiferromagnetic GdB_6 nanocrystals (~10 nm) embedded in an amorphous ferromagnetic matrix of $Gd_{73.5}Si_{13}B_{13.5}$ microwires from a controlled melt-extraction process [33]. Accordingly, it is possible to create Gd_3Ni nanocrystals within an amorphous $Gd_{65}Ni_{35}$ microwire to form a novel composite with enhanced magnetocaloric properties. Indeed, in related work, it was shown that a Gd_3Ni nanocrystalline phase was generated within $Gd_{65}Ni_{35}$ amorphous ribbons [13]. With this in mind, our group noted a report that crystalline (bulk) Gd_3Ni exhibited an AFM ordering at T_N ~ 99 K [37] and this T_N is expected to shift to a lower temperature in $Gd_3Ni/Gd_{65}Ni_{35}$ microwires due to significant AFM weakening in the Gd_3Ni phase caused by nanoscale size effects.

In this work, we demonstrate that controlled solidification of the melt-extraction process can create a novel class of biphase nanocrystalline/amorphous composite microwires comprising AFM Gd_3Ni nanocrystals embedded in an amorphous FM $Gd_{65}Ni_{35}$ matrix for enhanced MCE and RC without thermal annealing.

2. Experimental

The $Gd_3Ni/Gd_{65}Ni_{35}$ microwires were fabricated on a spinning copper wheel of 160 mm in diameter with a 60° tapered edge using the modified melt-extraction method. The wheel was kept at a fixed rotation speed of 30 m/min while the melted material was fed onto the wheel at a constant rate of 30 μm/s to obtain uniform dimensions in the melt-extracted wires. Energy dispersive X-ray spectroscopy (EDS) and scanning electron microscopy (SEM) were performed with a JSM-6390LV model from JEOL and INCA x-sight by OXFORD instruments. The microstructural evolution of the wires was further characterized by electron transmission microscopy (TEM) and selected area electron diffraction (SAED). The magnetic properties of $Gd_3Ni/Gd_{65}Ni_{35}$ wires with diameter $d \sim 45$ μm and length $l \sim 3$ mm were measured by a commercial Physical Property Measurement System (PPMS) by Quantum Design with a VSM option. DC magnetic fields of up to 5 T were applied longitudinally along the wire as the temperature was varied from 20 K to 180 K with an increment of 2 K.

3. Results and discussion

3.1. Structural properties

The micromorphology of a melt-extracted $Gd_3Ni/Gd_{65}Ni_{35}$ microwire was obtained by SEM, and the images demonstrate a smooth and homogeneous surface (Fig. 1a). The average diameter of the cylindrical microwire was identified directly from planar SEM images to be ~45 μm with a circular cross section. A typical EDS spectrum measured at room temperature is shown in Fig. 1b, which confirms the presence and quantitative mixing ratio of the two raw chemical elements Gd and Ni in the sample. The atomic percentages calculated by EDS were ~66% and ~34% for Gd and Ni, respectively, which allowed us to estimate the relative abundance of two constituent phases (Gd_3Ni and $Gd_{65}Ni_{35}$, as revealed by TEM and SAED below) in the microwire. If we consider ~10% abundance of Gd_3Ni and ~90% abundance of $Gd_{65}Ni_{35}$, then a simple calculation yields $(0.1 \times 75\%) + (0.9 \times 65\%) = 66\%$ Gd and $(0.1 \times 25\%) + (0.9 \times 35\%) = 34\%$ Ni.

The structural properties of the melt-extracted $Gd_3Ni/Gd_{65}Ni_{35}$ microwires were further characterized by XRD, TEM, and SAED. The results are displayed in Fig. 1c (XRD), inset of Fig. 1a (TEM), and inset of Fig. 1b (SAED). The XRD spectrum determined from 20° to 80° (2θ) with a scanning speed of 0.9°/min is shown Fig. 1c. A typical broad halo pattern with a broad diffuse peak is detected in the 2θ region between 20° and 40°. This broad peak in the XRD spectrum has also been observed for previously studied Gd-based microwires [18–28,30,31,33] and confirms the amorphous characteristic of $Gd_{65}Ni_{35}$. It is worth mentioning here that some detected crystalline peaks match the XRD peaks of Gd_3Ni nanocrystals [13]. Thus, TEM and SAED measurements were performed

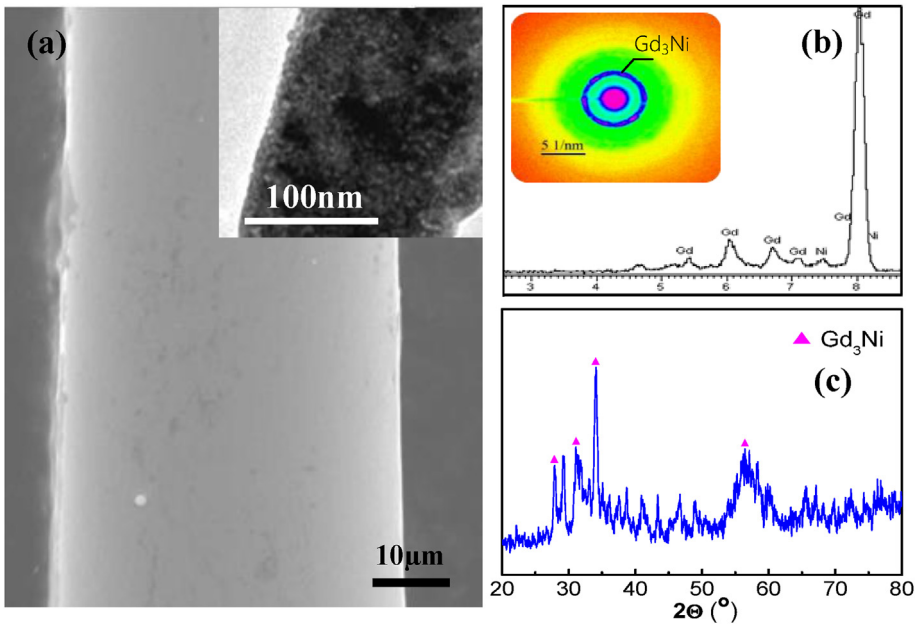

Fig. 1. (a) SEM image with an inset showing the TEM morphology; (b) energy dispersive spectroscopy (EDS) of the local region in the TEM image and the inset showing selected area electron diffraction (SAED) of the nanocrystalline microstructure including Gd_3Ni phase; and (c) X-ray diffraction pattern (XRD) of the $Gd_3Ni/Gd_{65}Ni_{35}$ microwires.

to confirm the presence of the Gd_3Ni nanocrystals. The results of TEM and SAED are shown in the inset of Fig. 1a and the inset of Fig. 1b. Indeed, both TEM and SAED confirmed that Gd_3Ni nanocrystals of ~8 nm diameter were embedded in a $Gd_{65}Ni_{35}$ amorphous matrix. A combination of these two phases is expected to be magnetically coupled with each other, thus affecting the magnetic and magnetocaloric properties over the entire microwire.

3.2. Magnetic properties

The temperature dependence of the magnetization $M(T)$ for all specimens of the $Gd_3Ni/Gd_{65}Ni_{35}$ composite wire was measured while cooling under an applied DC magnetic field of $\mu_0 H = 0.1$ T across a paramagnetic to ferromagnetic (PM-FM) phase transition. The results of a typical $M(T)$ curve is displayed in Fig. 2a. As can be seen clearly in Fig. 2a, the $M(T)$ curve exposes a broadened PM-FM phase transition around the Curie temperature T_C. This broadening is not only a typical characteristic of SOMT materials and caused by structural disorder of the amorphous material, but also due to the existence of two magnetic phases (e.g., the nanocrystalline Gd_3Ni and amorphous $Gd_{65}Ni_{35}$ phases) [32]. While the feature associated with the AFM ordering of the Gd_3Ni phase is not obviously seen on the M-T curve (Fig. 2), a small, broad peak associated with it at ~50 K from the $-\Delta S_M(T)$ curves is observed below (Fig. 3a). The Curie temperature (T_C) of the $Gd_3Ni/Gd_{65}Ni_{35}$ microwire determined from the minimum in dM/dT is ~120 K (see inset of Fig. 2a). The T_C value of the $Gd_3Ni/Gd_{65}Ni_{35}$ microwire in this study is similar to that reported for the $Gd_{65}Ni_{35}$ amorphous ribbon (T_C ~122 K) [13]. This T_C value is much higher than those reported for $Gd_{55}Ni_xAl_{45-x}$ bulk metallic alloys (T_C ~ 50–70 K for x = 15, 20, 25, and 30) [11].

To further understand the magnetic behavior of the $Gd_3Ni/Gd_{65}Ni_{35}$ microwire in the PM regime, the inverse susceptibility as a function of temperature, $\chi^{-1}(T) = \mu_o H/M$, generated from the $M(T)$ curve in the paramagnetic region, is provided in Fig. 2a. Its linear temperature dependence is consistent with the Curie–Weiss law in the paramagnetic region, $\chi = \frac{C}{T-\theta}$, where C is the Curie constant defined as $C = \frac{N_A \mu_B^2}{3k_B}\mu_{eff}^2$ (N_A = 6.022 × 10^{23} mol^{-1} is Avogadro number, μ_B = 9.274 × 10^{-21} emu is the Bohr magneton, and $k_B = 1.38016 \times 10^{-16}$ erg/K is the Boltzmann constant). A linear fit of $\chi^{-1}(T)$ yields θ = 124 K and C = 7.89 emu K mol^{-1} T^{-1}. The paramagnetic Curie temperature or Weiss temperature, θ = 124 K, is a positive value, which confirms the PM-FM phase transition. Additionally, this Weiss temperature θ is very close to the Curie temperature T_C (~120 K). This is likely associated with the presence of short-range magnetic order above T_C in the PM regime.

The effective magnetic moment μ_{eff} of the sample is determined from C via the following equation $\mu_{eff} = \sqrt{\frac{3k_B C}{N_A}} = \sqrt{8C}$. From this relationship, we obtained μ_{eff} = 7.941 μ_B for the $Gd_3Ni/Gd_{65}Ni_{35}$ microwires fabricated for this study. This μ_{eff} value is approximately equal to the theoretical value of pure Gd (~7.94 μ_B). Some previous studies reported similar values of μ_{eff} for Gd–Ni [38–41]. Paulose et al. [38], Mallik *et al.* [39], and Uhlirova *et al.* [40] suggested the parallel orientation of Gd and Ni moments as an explanation. However, an AFM coupling between the Gd and Ni moments was reported by Yano *et al.* [41]. In this work, the μ_{eff} value of the $Gd_3Ni/Gd_{65}Ni_{35}$ microwire is very close to that of pure Gd in the PM regime, but it is much smaller at temperatures below T_C. This could be attributed to the presence of AFM coupling between Gd and Ni moments and the additional presence of the AFM interaction of the Gd_3Ni phase.

Fig. 2b presents the temperature dependence of magnetization at different applied magnetic fields, the $M(T)$ curves, from $\mu_0 H$ = 0.1–5 T. The PM-FM phase transition becomes broadened with increasing applied magnetic field up, which is a typical behavior for SOMT materials. The largest changes in M with respect to T appear in a region from 120 K to 130 K, where T_C has been calculated from the minimum of the dM/dT and indicates that the largest changes in magnetic entropy will occur in this temperature region [27].

To investigate the magnetocaloric properties of the $Gd_3Ni/Gd_{65}Ni_{35}$ microwires, we measured a set of isothermal magnetization curves $M(\mu_0 H)$ at various temperatures around the Curie temperature ranging from 20 K to 180 K with a temperature step of 10 K up to a maximum applied DC magnetic field $\mu_0 H$ = 5 T, as

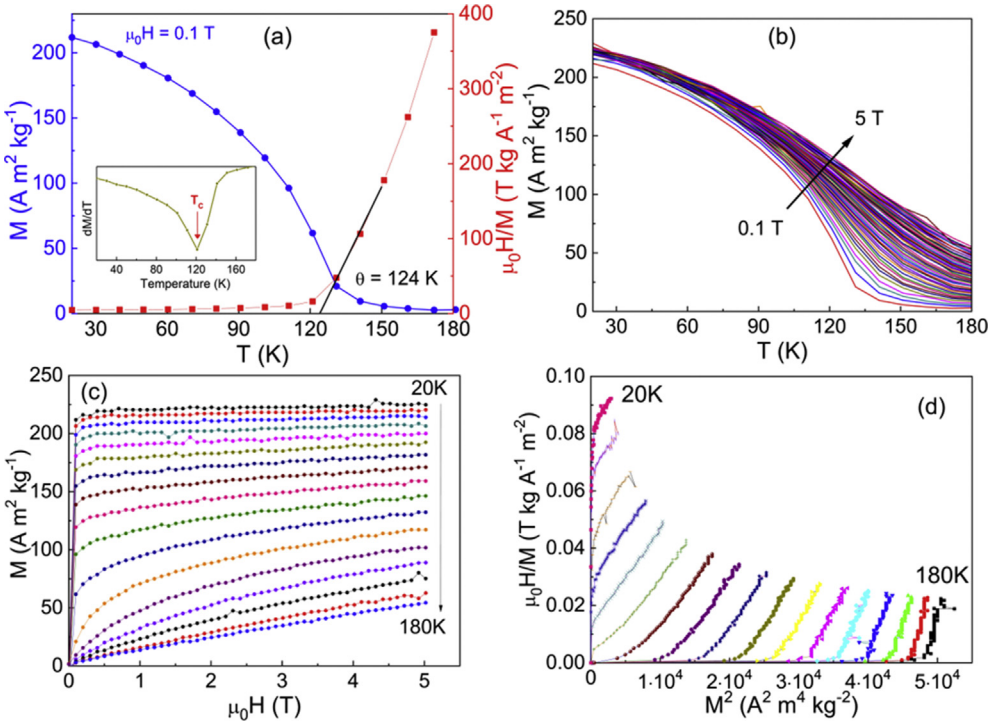

Fig. 2. (a) Temperature dependence of magnetization $M(T)$ and its derivative (dM/dT) taken in a field of 0.1 T for the $Gd_3Ni/Gd_{65}Ni_{35}$ microwires; (b) temperature and magnetic field dependence of the magnetization; (c) magnetic field dependence of magnetization $M(H)$ taken at temperatures around the Curie temperature; and (d) Arrott plots ($\mu_0 H/M$ vs. M^2) of the $Gd_3Ni/Gd_{65}Ni_{35}$ microwires.

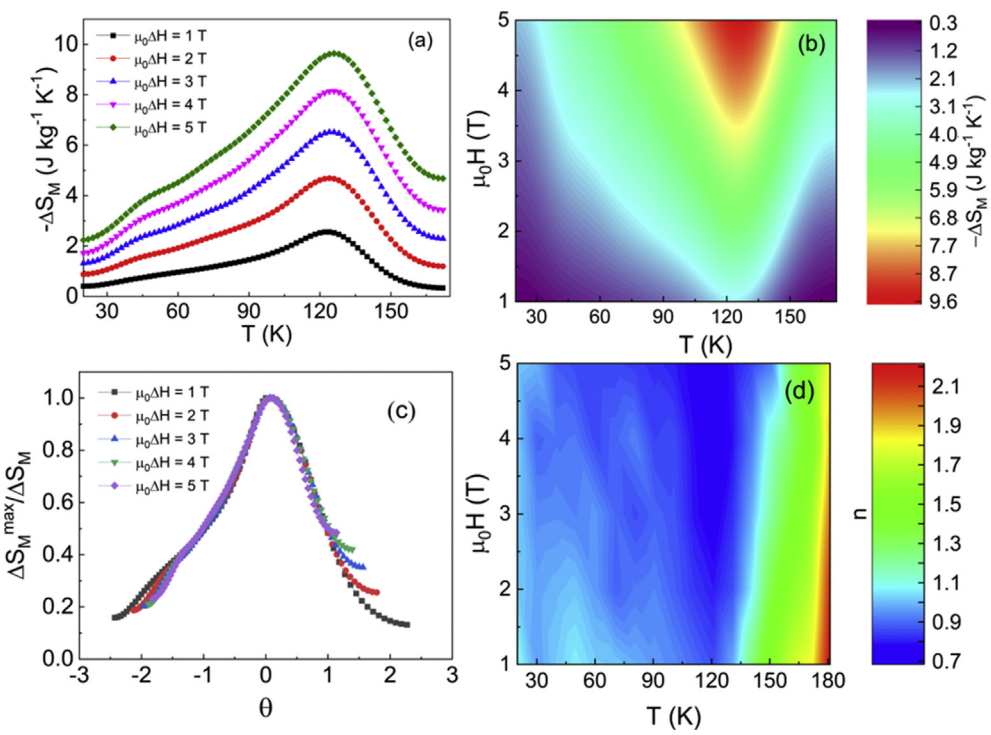

Fig. 3. (a) Temperature dependence of magnetic entropy change $-\Delta S_M(T)$ of the $Gd_3Ni/Gd_{65}Ni_{35}$ microwires for selected magnetic field changes; (b) the filled 2D contour plot of the temperature and field dependence of the magnetic entropy change; (c) the universal $\Delta S_M/\Delta S_M^{max}$ curve; and (d) temperature dependence of the local exponent (n) confirming the field dependence of $-\Delta S_M(T)$ of the $Gd_3Ni/Gd_{65}Ni_{35}$ microwires for different maximum applied fields.

exhibited in Fig. 2c. After that, to confirm the nature of the PM-FM phase transition of the $Gd_3Ni/Gd_{65}Ni_{35}$ microwires, these curves were converted into Arrott plots (μ_0H/M vs. M^2). The curves obtained from that transformation are shown in Fig. 2d. Conforming to the Banerjee criterion [42], a PM-FM magnetic phase transition is considered a first-order magnetic transition (FOMT) when the slope of μ_0H/M vs. M^2 is negative; in contrast, it is considered to be a SOMT when the slope of the Arrott plot is positive. As can be seen clearly in Fig. 2d, all slopes of the re-scaled isotherms are uniformly positive, which indicates that the PM-FM phase transition of the $Gd_3Ni/Gd_{65}Ni_{35}$ microwires is a type of SOMT. This result is in agreement with our previous reports on Gd-based microwires [15–30,33].

3.3. Magnetocaloric effect

From the $M(\mu_0H)$ curves of the $Gd_3Ni/Gd_{65}Ni_{35}$ microwire, the magnetic entropy change $-\Delta S_M$ due to an applied magnetic field change between 0 and H_{max} was calculated using the thermodynamic Maxwell relation [1]:

$$\Delta S_M(T,\mu_o H) = \mu_0 \int_0^{H_{max}} \left(\frac{\partial M}{\partial T}\right)_H dH, \quad (1)$$

where M is the magnetization, μ_oH is the applied magnetic field, and T is the temperature.

Fig. 3a exhibits the temperature dependence of $-\Delta S_M$ in applied magnetic field (μ_oH) ranging from 0 to 5 T for the $Gd_3Ni/Gd_{65}Ni_{35}$ microwires. A contour color plot $-\Delta S_M(T,\mu_oH)$ is also displayed in Fig. 3b for the purpose of focusing attention on the broadening of the $-\Delta S_M(T,\mu_oH)$ curves across the PM-FM phase transition. As can be seen in Fig. 3a, the magnitude of $-\Delta S_M$ increases with an increase in μ_oH and the maximum of $-\Delta S_M$ occurs near the T_C as expected. For an applied field change of 5 T, a large maximum value of $|\Delta S_M|$ was calculated to be ~9.64 J/kg K at ~120 K. Compared with the previous study, this $|\Delta S_M|$ value is 1.4 times larger than that detected in the $Gd_{65}Ni_{35}$ ribbon sample [13]. It is worth noting that in addition to the dominant peak of the $-\Delta S_M(T)$ curves associated with the PM-FM phase transition at T_C ~120 K, a small, broad peak around ~50 K was also observed and attributed to the AFM transition of the nanocrystalline Gd_3Ni phase. Since this AFM phase is considerably weak at the nanoscale, application of a sufficiently high magnetic field may convert it into FM and give rise to the broad $-\Delta S_M(T)$ curve and hence the large RC – an important figure of merit in magnetic cooling.

To confirm the SOMT of the PM-FM phase transition, in addition to Banerjee's criterion-based Arrott plots, another method based on the universal curve of $-\Delta S_M(T)$ was used as demonstrated by Franco et al. [45]. Following this method, $-\Delta S_M$ is normalized to $-\Delta S_M^{max}$ and the T axis is rescaled as $\theta = \frac{(T-T_C)}{T_{r2}-T_C}(T \geq T)_C$ or $\theta = -\frac{(T-T_C)}{T_{r1}-T_C}$ $(T \leq T_C)$, where T_{r1} and T_{r2} are two reference temperatures above and below T_C satisfying the relation $\Delta S_M(T_{r1}) = \Delta S_M(T_{r1}) = f \times \Delta S_M^{max}$ ($f = 0.5$ for this study). For SOMT, all the $-\Delta S_M(T)$ curves obtained at various applied magnetic fields μ_oH must collapse onto a universal curve. Fig. 3c displays the master universal curve $\Delta S_M/\Delta S_M^{max}$ versus θ curve for $\mu_oH = 1$–5 T. It once again proves that a SOMT exists in the $Gd_3Ni/Gd_{65}Ni_{35}$ microwires, which is fully consistent with Banerjee's criterion.

As discussed above, $-\Delta S_M$ depends on the temperature, T, at a constant applied magnetic field μ_oH. Moreover, $-\Delta S_M$ is a function of the maximum magnetic field, μ_oH, which can be expressed as

$$\Delta S_M \propto \mu_0 H^n \quad (2)$$

For all the $-\Delta S_M$ curves, where n is the local exponent dependent on the magnetic state of the material [45]. At the peak of the magnetic entropy change or at T_C, the exponent n is independent of the change in μ_oH. In temperature ranges above T_C and below T_C, the field dependence of the magnetic entropy change indicates a quadratic and a first-order dependence, respectively, in the PM and FM regime, respectively. This means that at temperatures far away from T_C, n will asymptotically reach 1 or 2, respectively, as T is far below or above T_C, respectively. To clarify the magnetic field dependence of $-\Delta S_M$, n can be determined by the following equation:

$$n = \frac{d(ln|\Delta S_M|)}{d(lnH)} \quad (3)$$

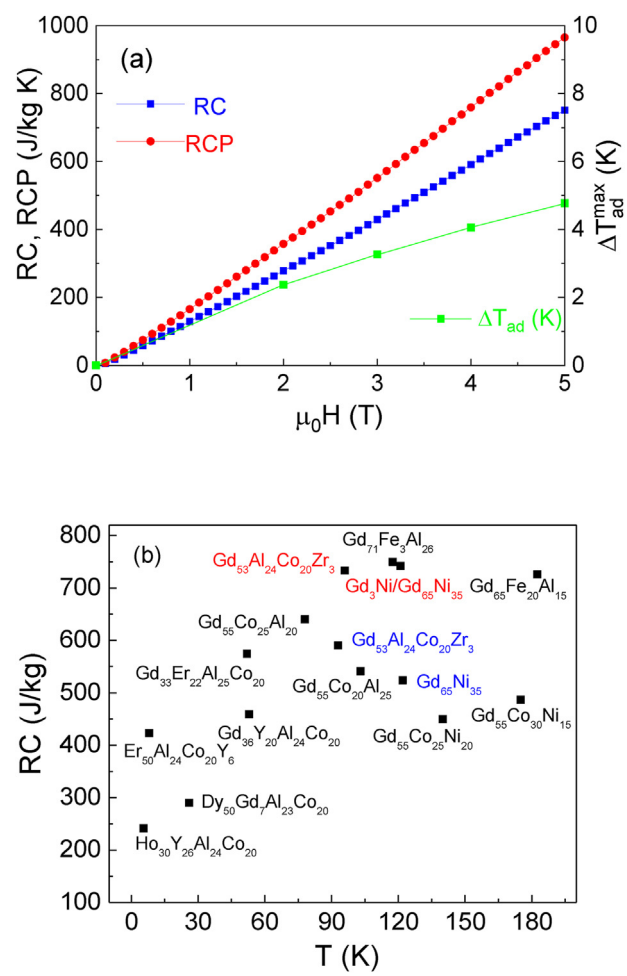

Fig. 4. (a) (left, blue and red) Magnetic field dependence of the refrigerant capacity (RC) and the relative power capacity (RCP) of the $Gd_3Ni/Gd_{65}Ni_{35}$ microwires and (right, green) magnetic field dependence of the maximum adiabatic temperature change ΔT_{ad}^{max} at T_C for the $Gd_3Ni/Gd_{65}Ni_{35}$ microwires; (b) RC values of magnetocaloric candidate materials in the temperature range of 10–200 K. Red indicates the microwires, while blue indicates their bulk counterparts for a one-to-one comparison.

Fig. 3d displays the temperature dependence of n for the $Gd_3Ni/Gd_{65}Ni_{35}$ microwires for $\mu_0H = 1, 2, 3, 4$, and 5 T in a 2D surface plot. As can be seen in Fig. 3d, in the PM regime and far above T_C, n approaches 2, while in the FM regime and far below T_C, n approaches 1 as expected. Nevertheless, at temperatures near T_C, the n value is approximately 0.7–0.86. According to Oestrreicher et al. [46], if the n exponent at the Curie temperature is close to 2/3 (~0.67), it corresponds to the mean field model. For the $Gd_3Ni/Gd_{65}Ni_{35}$ microwires, n ~0.70–0.86, which is slightly higher than that of the mean field model (~0.67). This deviation is likely due to complex magnetic interactions caused by structural disorder in the amorphous $Gd_{65}Ni_{35}$ matrix [15–30] and the presence of Gd_3Ni nanocrystals embedded in this amorphous matrix. Another notable point here is that the value of n has a small change corresponding to the change of the applied magnetic field at the T_C (0.7–0.86 for 1 T–5 T, respectively). The local exponent n is field independent at T_C for single-phase SOMT materials, but it can decay with the change of μ_0H for multiphase magnetic systems, such as the present $Gd_3Ni/Gd_{65}Ni_{35}$ microwires [7,47].

To evaluate the adiabatic temperature rise, ΔT_{ad}, the specific heat capacity was measured as a function of temperature in applied magnetic fields of 0, 2, and 5 T for the $Gd_3Ni/Gd_{65}Ni_{35}$ microwires [48]. Accordingly, we have estimated the maximum adiabatic temperature change ΔT_{ad}^{max} at T_C using the following equation [2]:

$$\Delta T_{ad}(T_C, H_0) = -\Delta S_M(T_C, H_0) \cdot \frac{T_C}{C(T_C, H_0)_P}, \tag{4}$$

where $C(T,H_0)$ is the heat capacity.

Fig. 4a (right side, green) shows the applied magnetic field dependence of ΔT_{ad}^{max} for the $Gd_3Ni/Gd_{65}Ni_{35}$ microwires. For $\mu_0H = 5$ T, the ΔT_{ad}^{max} value is approximately equal to 4.77 K. We also estimated ΔT_{ad}^{max} at magnetic fields of 2 T, 3 T, and 4 T, and the results obtained are 2.37 K, 3.26 K, and 4.05 K, respectively. These values are comparable with those reported for Gd-Al-Co microwires [31] and are promising for applications in magnetic refrigeration.

The RC of the $Gd_3Ni/Gd_{65}Ni_{35}$ microwires has been calculated from the data by integrating the area under the $-\Delta S_M$-T curves by using the temperatures at half maximum of the peaks in the following way:

$$RC = \int_{T_{hot}}^{T_{cold}} -\Delta S_M(T)\mathrm{d}T, \tag{5}$$

where T_{cold} and T_{hot} are the onset and offset temperatures of δT_{FWHM}, respectively. The other method, using the relative cooling power (RCP), represents an amount of heat transfer between the hot and cold sides in an ideal refrigeration cycle, which is defined as Wood and Potter's method:

$$RCP = -\Delta S_M^{max}\ \delta T_{FWHM}, \tag{6}$$

where $\delta T_{FWHM} = T_{hot} - T_{cold}$ is the temperature difference at the full width at half maximum of the -$\Delta S_M(T)$ curve. The RC value increased significantly with increasing applied magnetic field, which was similar to the magnetic field dependence of RCP. Values of RC and RCP are plotted as functions of magnetic field as shown in Fig. 4a. For comparison, the RC and RCP values of the present microwires and other candidate materials for a field change of 5 T are summarized in Table 1 and selectively plotted in Fig. 4b. For $\mu_0H = 5$ T, the RC and RCP values for the $Gd_3Ni/Gd_{65}Ni_{35}$ microwires are calculated to be ~751 J/kg and ~965 J/kg, respectively. This RC value is 40% higher than that of the $Gd_{65}Ni_{35}$ ribbon (~524 J/kg) [13]. As one can see clearly from Table 1, the $Gd_3Ni/Gd_{65}Ni_{35}$ microwires almost have the largest RC and RCP among the compared candidates. While the RC value of the $Gd_3Ni/Gd_{65}Ni_{35}$

Table 1
Comparison of the magnetocaloric characteristics of the $Gd_3Ni/Gd_{65}Ni_{35}$ composite microwires and other MCE materials with reference to their phase structures.

Material	Structure	T_C (K)	-ΔS_M (J/kg K)	RC (J/kg)	RCP (J/kg)	Applied Field (T)	Reference
$Gd_3Ni/Gd_{65}Ni_{35}$	AM + NC	121	9.64	751	965.3	5	This work
$Gd_{65}Ni_{35}$	GR	122	6.9	524	–	5	[13]
$GdB_6/Gd_{73.5}Si_{13}B_{13.5}$	AM + NC	106	6.4	790	885	5	[33]
$Gd_{50}Al_{30}Co_{20}$	AM + NC	86	10.09	672	861	5	[31]
$Gd_{55}Al_{25}Co_{20}$	AM + NC	100	9.67	652	861	5	[21]
$Gd_{60}Al_{20}Co_{20}$	AM + NC	109	10.11	681	915	5	[20]
$Gd_{53}Al_{24}Co_{20}Zr_3$ (Annealed at 100 °C)	AM + NC	94	9.5	687	893	5	[32]
$Gd_{53}Al_{24}Co_{20}Zr_3$ (Annealed at 200 °C)	AM + NC	94	8.0	629	744	5	[32]
$Gd_{53}Al_{24}Co_{20}Zr_3$ (Annealed at 300 °C)	AM + NC	94	5.1	396	525	5	[32]
$Gd_{60}Al_{25}Co_{15}$	AM	101	9.73	732	973	5	[22]
$Gd_{55}Al_{20}Co_{25}$	AM	110	9.69	580	804	5	[23]
Gd_{50}-$(Co_{69.25}Fe_{4.25}Si_{13}B_{13.5})_{50}$	AM	170	6.56	625	826	5	[24]
Gd_{50}-$(Co_{69.25}Fe_{4.25}Si_{13}B_{13.5})_{50}$	AM	174	5.90	–	–	5	[26]
$Gd_{60}Fe_{20}Al_{20}$	AM	202	4.8	687	900	5	[27]
$Gd_{59.4}Al_{19.8}Co_{19.8}Fe_1$	AW	113	10.33	748.22	1006	5	[25]
$Gd_{53}Al_{24}Co_{20}Zr_3$	MW	96	10.3	733.4	–	5	[15]
$Gd_{55}Co_{25}Ni_{20}$	GR	140	6.04	450	–	5	[14]
$Gd_{55}Co_{30}Ni_{15}$	GR	175	6.3	487	–	5	[14]
$Gd_{55}Co_{20}Al_{25}$	BMG	103	8.8	541	–	5	[10]
$Gd_{55}Ni_{25}Al_{20}$	BMG	78	8	640	–	5	[10]
$Gd_{53}Al_{24}Co_{20}Zr_3$	BMG	93	9.4	590	–	5	[9]
$Gd_{33}Er_{22}Al_{25}Co_{20}$	BMG	52	9.47	574	–	5	[9]
$Ho_{30}Y_{26}Al_{24}Co_{20}$	BMG	5.5	10.76	241	–	5	[43]
$Dy_{50}Gd_7Al_{23}Co_{20}$	BMG	26	9.77	290	–	5	[43]
$Er_{50}Al_{24}Co_{20}Y_6$	BMG	8	15.91	423	–	5	[43]
$Gd_{71}Fe_3Al_{26}$	BMG	117.5	7.4	750	–	5	[12]
$Gd_{65}Fe_{20}Al_{15}$	BMG	182.5	5.8	726	–	5	[12]
$Gd_{36}Y_{20}Al_{24}Co_{20}$	BMG	53	7.76	459	–	5	[44]

AM: Amorphous Microwires, NC: Nanocrystals, GR: Glassy Ribbon, BMG: Bulk Metallic Glass.

microwires is nearly equal to that of $Gd_{53}Al_{24}Co_{20}Zr_3$ microwires (733 J/kg), the T_C of the former (~120 K) is significantly higher than that of the latter (96 K). The present $Gd_3Ni/Gd_{65}Ni_{35}$ microwires are therefore more advantageous for magnetic refrigeration in the liquid nitrogen temperature regime. In general, magnetocaloric microwires with AM/AM + NC structures represent significantly higher RC and RCP values relative to their RG/BMG counterparts [31–33].

4. Conclusion

In summary, we have shown that a novel biphase nanocrystalline/amorphous structure can be created in Gd alloy microwires, such as $Gd_3Ni/Gd_{65}Ni_{35}$ microwires, directly from melt extraction through controlled solidification. The $Gd_3Ni/Gd_{65}Ni_{35}$ microwires show higher Curie temperature and larger RC as compared to their bulk and ribbon counterparts. These excellent magnetocaloric characteristics make the microwires in this study an attractive candidate material for applications as a cooling device for micro- and nano-scale electromechanical systems.

Declaration of competing interest

The authors declare that they have no known competing financial interests or personal relationships that could have appeared to influence the work reported in this paper.

Acknowledgments

Work at USF was supported by the U.S. Department of Energy, Office of Basic Energy Sciences, Division of Materials Sciences and Engineering under Award No. DE-FG02-07ER 46438 (Magnetocaloric studies). Work at HIT was supported by the National Natural Science Foundation of China NSFC, (Nos. 51671071) (Sample fabrication and TEM characterization). Work at ZJU was supported by the National Natural Science Foundation of China NSFC, (Nos. 51671171). The research work at Korea was supported by the National Research Foundation of Korea under Grant No: 2020R1A2C1008115 (Magnetic measurements). The authors thank Dr. Tatiana Eggers for proofreading this manuscript.

References

[1] V. Franco, J.S. Blazquez, B. Ingale, A. Conde, The magnetocaloric effect and magnetic refrigeration near room temperature: materials and models, Annu. Rev. Mater. Res. 42 (2012) 305.
[2] M.H. Phan, S.C. Yu, Review of the magnetocaloric effect in manganite materials, J. Magn. Magn. Mater. 308 (2007) 325.
[3] V. Franco, J.S. Blazquez, J.J. Ipus, J.Y. Law, L.M. Moreno-Ramirez, A. Conde, Magnetocaloric effect: from materials research to refrigeration devices, Prog. Mater. Sci. 93 (2018) 112.
[4] N.S. Bingham, M.H. Phan, H. Srikanth, M.A. Torija, C. Leighton, Magnetocaloric effect and refrigerant capacity in charge-ordered manganites, J. Appl. Phys. 106 (2009), 023909.
[5] P. Lampen, N.S. Bingham, M.H. Phan, H. Kim, M. Osofsky, A. Piqué, T.L. Phan, S.C. Yu, H. Srikanth, Impact of reduced dimensionality on the magnetic and magnetocaloric response of $La_{0.7}Ca_{0.3}MnO_3$, Appl. Phys. Lett. 102 (2013), 062414.
[6] A. Biswas, S. Chandra, T. Samanta, B. Ghosh, S. Datta, M.H. Phan, A.K. Raychaudhuri, I. Das, H. Srikanth, Universality in the entropy change for the inverse magnetocaloric effect, Phys. Rev. B 87 (2013) 134420.
[7] M.H. Phan, V. Franco, A. Chaturvedi, S. Stefanoski, G.S. Nolas, H. Srikanth, Origin of the magnetic anomaly and tunneling effect of europium on the ferromagnetic ordering in $Eu_{8-x}Sr_xGa_{16}Ge_{30}$ (x=0,4) type-I clathrates, Phys. Rev. B 84 (2011), 054436.
[8] J. Liu, T. Gottschall, K.P. Skokov, J.D. Moore, O. Gutfleisch, Giant magnetocaloric effect driven by structural transitions, Nat. Mater. 11 (2012) 620.
[9] Q. Luo, D.Q. Zhao, M.X. Pan, W.H. Wang, Magnetocaloric effect in Gd-based bulk metallic glasses, Appl. Phys. Lett. 89 (2006), 081914.
[10] J. Du, Q. Zheng, Y.B. Li, Q. Zhang, D. Li, Z.D. Zhang, Large magnetocaloric effect and enhanced magnetic refrigeration in ternary Gd-based bulk metallic glasses, J. Appl. Phys. 103 (2008), 023918.
[11] F. Yuan, J. Du, B. Shen, Controllable spin-glass behavior and large magnetocaloric effect in Gd-Ni-Al bulk metallic glasses, Appl. Phys. Lett. 101 (2012), 032405.
[12] Q.Y. Dong, B.G. Shen, J. Chen, J. Shen, F. Wang, H.W. Zhang, J.R. Sun, Large magnetic refrigerant capacity in $Gd_{71}Fe_3Al_{26}$ and $Gd_{65}Fe_{20}Al_{15}$ amorphous alloys, J. Appl. Phys. 105 (2009), 053908.
[13] X.C. Zhong, P.F. Tang, Z.W. Liu, D.C. Zeng, Z.G. Zheng, H.Y. Yu, W.Q. Qiu, M. Zou, Magnetic properties and large magnetocaloric effect in Gd–Ni amorphous ribbons for magnetic refrigeration applications in intermediate temperature range, J. Alloy. Compd. 509 (2011) 6889–6892.
[14] X.C. Zhong, P.F. Tang, Z.W. Liu, D.C. Zeng, Z.G. Zheng, H.Y. Yu, W.Q. Qiu, H. Zhang, R.V. Ramanujan, Large magnetocaloric effect and refrigerant capacity in Gd-Co-Ni metallic glasses, J. Appl. Phys. 111 (2012), 07A919.
[15] N.S. Bingham, H. Wang, F. Qin, H.X. Peng, J.F. Sun, V. Franco, H. Srikanth, M.H. Phan, Excellent magnetocaloric properties of melt-extracted Gd-based amorphous microwires, Appl. Phys. Lett. 101 (2012) 102407.
[16] F.X. Qin, N.S. Bingham, H. Wang, H.X. Peng, J.F. Sun, V. Franco, S.C. Yu, H. Srikanth, M.H. Phan, Mechanical and magnetocaloric properties of Gd based amorphous microwires fabricated by melt-extraction, Acta Mater. 61 (2013) 1284–1293.
[17] A. Biswas, Y.Y. Yu, N.S. Bingham, H. Wang, F.X. Qin, J.F. Sun, S.C. Yu, V. Franco, H. Srikanth, M.H. Phan, Impact of structural disorder on the magnetic ordering and magnetocaloric response of amorphous Gd-based microwires, J. Appl. Phys. 115 (2014) 17A318.
[18] H. Wang, D. Xing, X. Wang, J. Sun, Fabrication and characterization of melt-extracted Co-based amorphous wires, Metall. Mater. Trans. 42 (2010) 1103–1108.
[19] H. Wang, F.X. Qin, D.W. Xing, F.Y. Cao, X.D. Wang, H.X. Peng, J.F. Sun, Relating residual stress and microstructure to mechanical and giant magneto-impedance properties in cold-drawn Co-based amorphous microwires, Acta Mater. 60 (2012) 5425–5436.
[20] H.X. Shen, H. Wang, L. Jingshun, F. Cao, F. Qin, D. Xing, D. Chen, Y. Liu, J. Sun, Enhanced magnetocaloric properties of melt-extracted GdAlCo metallic glass microwires, J. Magn. Magn. Mater. 372 (2014) 23–26.
[21] H.X. Shen, H. Wang, J. Liu, D. Xing, F. Qin, F. Cao, D. Chen, Y. Liu, J. Sun, Enhanced magnetocaloric and mechanical properties of melt-extracted $Gd_{55}Al_{25}Co_{20}$ micro-fibers, J. Alloy. Compd. 603 (2014) 167–171.
[22] D. Xing, H. Shen, S. Jiang, J. Liu, M.H. Phan, H. Wang, F. Qin, D. Chen, Y. Liu, J. Sun, Magnetocaloric effect and critical behavior in melt-extracted $Gd_{60}Co_{15}Al_{25}$ microwires, Phys. Stat. Sol. 212 (2015) 1905–1910.
[23] D. Xing, H. Shen, J. Liu, H. Wang, F. Cao, F. Qin, D. Chen, Y. Liu, J. Sun, Magnetocaloric effect in uncoated $Gd_{55}Al_{20}Co_{25}$ amorphous wires, Mater. Res. 18 (2015) 49–54.
[24] Y. Bao, H. Shen, D. Xing, S. Jiang, J. Sun, M.H. Phan, Enhanced Curie temperature and cooling efficiency in melt-extracted $Gd_{50}(Co_{69.25}Fe_{4.25}Si_{13}B_{13.5})_{50}$ microwires, J. Alloy. Compd. 708 (2017) 678–684.
[25] J. Liu, Q. Wang, M. Wu, Y. Zhang, H. Shen, W. Ma, Improving the refrigeration capacity of Gd-rich wires through Fe-doping, J. Alloy. Compd. 711 (2017) 71–76.
[26] N.T.M. Duc, H.X. Shen, E. Clements, O. Thiabgoh, J.L. Sanchez Llamazarese, C.F. Sanchez-Valdes, N.T. Huong, J.F. Sund, H. Srikanth, M.H. Phan, Critical magnetic and magnetocaloric behavior of amorphous melt-extracted $Gd_{50}(Co_{69.25}Fe_{4.25}Si_{13}B_{13.5})_{50}$ microwires, Intermetallics 110 (2019) 106479.
[27] N.T.M. Duc, H.X. Shen, E. Clements, O. Thiabgoh, J.L. Sanchez Llamazarese, C.F. Sanchez-Valdes, N.T. Huong, J.F. Sund, H. Srikanth, M.H. Phan, Enhanced refrigerant capacity and Curie temperature of amorphous $Gd_{60}Fe_{20}Al_{20}$ microwires, J. Alloy. Compd. 807 (2019) 151694.
[28] Y.F. Wang, F.X. Qin, Y.H. Wang, H. Wang, R. Das, M.H. Phan, H.X. Peng, Magnetocaloric effect of Gd-based microwires from binary to quaternary system, AIP Adv. 7 (2017), 056422.
[29] Y. Bao, H. Shen, Y. Huang, D. Xing, H. Wang, J. Liu, H. Li, H. Yin, S. Jiang, J. Sun, M.H. Phan, Table-like magnetocaloric behavior and enhanced cooling efficiency of a Bi-constituent Gd alloy wire-based composite, J. Alloy. Compd. 764 (2018) 789–793.
[30] H.X. Shen, L. Luo, Y. Bao, H. Yin, S. Jiang, L. Zhang, Y. Huang, S. Feng, D. Xing, J. Liu, Z. Li, Y. Liu, J. Sun, M.H. Phan, New DyHoCo medium entropy amorphous microwires of large magnetic entropy change, J. Alloy. Compd. 837 (2020) 155431.
[31] H.X. Shen, D.W. Xing, J.L. Sanchez Llamazares, C.F. Sanchez-Valdes, H. Belliveau, H. Wang, F.X. Qin, Y.F. Liu, J.F. Sun, H. Srikanth, M.H. Phan, Enhanced refrigerant capacity in Gd-Al-Co microwires with a biphase nanocrystalline/amorphous structure, Appl. Phys. Lett. 108 (2016), 092403.
[32] H.F. Belliveau, Y.Y. Yu, Y. Luo, F.X. Qin, H. Wang, H.X. Shen, J.F. Sun, S.C. Yu, H. Srikanth, M.H. Phan, Improving mechanical and magnetocaloric responses of amorphous melt-extracted Gd-based microwires via nanocrystallization, J. Alloy. Compd. 692 (2017) 658–664.
[33] N.T.M. Duc, H.X. Shen, O. Thiabgoh, N.T. Huong, J.F. Sun, M.H. Phan, Melt-extracted $Gd_{73.5}Si_{13}B_{13.5}/GdB_6$ ferromagnetic/antiferromagnetic microwires with excellent magnetocaloric properties, J. Alloy. Compd. 818 (2020) 153333.
[34] V.V. Khovaylo, V.V. Rodionoval, S.N. Shevyrtalov, V. Novosad, Magnetocaloric effect in "reduced" dimensions: thin films, ribbons, and microwires of Heusler alloys and related compounds, Phys. Stat. Sol. 251 (2014) 2104.
[35] M.D. Kuzmin, Factors limiting the operation frequency of magnetic refrigerators, Appl. Phys. Lett. 90 (2007) 251916.
[36] M.H. Phan, S. Chandra, N.S. Bingham, H. Srikanth, C.L. Zhang, S.W. Cheong, T.D. Hoang, H.D. Chinh, Collapse of charge ordering and enhancement of

magnetocaloric effect in nanocrystalline $La_{0.35}Pr_{0.275}Ca_{0.375}MnO_3$, Appl. Phys. Lett. 97 (2010) 242506.
[37] D.A. Shishkin, N.V. Baranov, A.V. Proshkin, S.V. Andreev, A.S. Volegov, Magnetic properties and magnetocaloric effect of Gd_3Ni in crystalline and amorphous states, Solid State Phenom. 190 (2012) 355–358.
[38] P.L. Paulose, S. Patil, R. Mallik, E.V. Sampathkumaran, V. Nagarajan, Ni3d-Gd4f correlation effects on the magnetic behaviour of GdNi, Phys. B 223–224 (1996) 382.
[39] R. Mallik, P.L. Paulose, E.V. Sampathkumaran, S. Patil, V. Nagarajan, Coexistence of localized and (induced) itinerant magnetism and heat-capacity anomalies in Gd1−xYxNi alloys, Phys. Rev. B 55 (1997) 8369.
[40] K. Uhlırova, J. Prokleskaa, J. Poltierova Vejpravova, V. Sechovsky, K. Maezawa, Magnetic and magnetoelastic properties of GdNi: single-crystal study, J. Magn. Magn. Mater. 310 (2007) 1753–1754.
[41] K. Yano, I. Umehara, K. Sato, A. Yaresko, Revelation of Ni magnetic moment in GdNi single crystal by soft X-ray magnetic circular dichroism, Solid State Commun. 136 (2005) 67–70.
[42] B.K. Banerjee, On a generalised approach to first and second order magnetic transitions, Phys. Lett. 12 (1964) 16–17.
[43] Q. Luo, D.Q. Zhao, M.X. Pan, W.H. Wang, Magnetocaloric effect of Ho-, Dy-, and Er-based bulk metallic glasses in helium and hydrogen liquefaction temperature range, Appl. Phys. Lett. 90 (2007) 211903.
[44] L. Liang, X. Hui, Y. Wu, G.L. Chen, Large magnetocaloric effect in $Gd_{36}Y_{20}Al_{24}Co_{20}$ bulk metallic glass, J. Alloy. Compd. 457 (2008) 541–544.
[45] V. Franco, J.S. Blázquez, M. Millán, J.M. Borrego, C.F. Conde, A. Conde, The magnetocaloric effect in soft magnetic amorphous alloys, J. Appl. Phys. 101 (2007), 09C503.
[46] H. Oestrreicher, F.T. Parker, Magnetic cooling near Curie temperatures above 300 K, J. Appl. Phys. 55 (1984) 12.
[47] V. Franco, R. Caballero-Flores, A. Conde, Q.Y. Dong, H.W. Zhang, The influence of a minority magnetic phase on the field dependence of the magnetocaloric effect, J. Magn. Magn. Mater. 321 (2019) 1115.
[48] H.F. Belliveau, Reduced Dimensionality Effects in Gd-Based Magnetocaloric Materials, PhD Dissertation, University of South Florida, 2016.